

## Synthesis, characterization and photocatalytic recital of nest-like zinc oxide photocatalyst

Sonali Prakashrao Chaudhari<sup>†</sup>, Anjali Babasaheb Bodade, and Gajanan Niranjanrao Chaudhari

Nano Technology Research Laboratory, Department of Chemistry, Shri Shivaji Science College,  
Amravati 444602, Maharashtra, India  
(Received 26 October 2012 • accepted 7 August 2013)

**Abstract**—3D nest-like ZnO nanostructures are synthesized via hydrothermal method operated at ambient temperature (80 °C). The as-synthesized ZnO nanostructures are assembled by numerous ultrathin nanosheets resulting into formation of many grooves which improved the photocatalytic property. The as-synthesized ZnO sample is characterized by XRD, FESEM, FT-IR, Raman spectra, BET surface area and photoluminescence spectra analysis. Moreover, the photocatalytic efficiency of as-synthesized ZnO nanostructures is evaluated for degradation of methylene blue (MB) dye degradation. A comparison with the commercial counterpart reveals that the as synthesized nest-like ZnO degrades MB dye more efficiently. The present synthetic method can provide an effective route for synthesis of other hierarchically structured metal oxides also.

Key words: ZnO, Hydrothermal Synthesis, Methylene Blue and Photocatalytic Properties

### INTRODUCTION

Zinc oxide (ZnO) is a well known polar II-VI semiconductor compound having iconicity at the borderline between the covalent and ionic semiconductors [1]. It is an intrinsic n-type semiconductor because of deviation from stoichiometry and the presence of intrinsic defects such as O vacancies ( $V_O$ ) and Zn interstitials ( $Zn_i$ ) [1]. ZnO is a semiconductor with wide band gap of 3.37 eV and large exciton binding energy of 60 meV. In terms of band energy, ZnO is a suitable alternative to TiO<sub>2</sub> [2]. ZnO is also an environmentally friendly material that does not form toxic byproducts [3]. It has received much research attention due to its low toxicity and low price, high chemical and thermal stability, high transparency in the visible wavelength range and unique optical properties. In powder form, ZnO is a very important material due to its potential applications in numerous areas such as electronics and photonics.

ZnO is a very promising photocatalyst for photocatalytic degradation of water pollutants such as phenol [4] and its derivatives [5] either under UV light [6] or sunlight [7]. Zinc oxide has been used in numerous applications, such as antireflection coatings [8], transparent electrodes in solar cells [9], varistors [10], light emitting diodes [11], gas sensors [12], acousto-optical devices [13], lasers [14], near-UV emissions [15], photocatalysis [16], antibacterial agents [17] and piezoelectric devices [18].

Various kinds of morphologies of ZnO including nanopins [19], nanorods [20], nanotubes [21], nanoscrews [22], nanowhisker [23], obelisk-like [24], tower-like, flower-like [25] and nanopencils [26] have been fabricated. Since different morphologies of ZnO show different electron emission, optical, electrical and acoustic properties, many efforts have been made to find the optimum fabrication process for ZnO with excellent properties [27]. Accordingly, many methods have been developed for the synthesis of ZnO. Most of

them are physical ones, such as thermal evaporation [28], chemical vapor deposition [29], pulsed laser deposition [30], metal-organic chemical vapor deposition [31] and molecular beam epitaxy [32]. Generally, instrumental methods require special and expensive equipment or operation control. Others include solution-based chemical methods such as solvothermal [33], sol-gel [34], sonochemical [35] and electrodeposition processes [36]. Among these, hydrothermal/solvothermal routes are very attractive because of the distinct advantages such as simplicity, low cost, mild synthesis conditions and potential for large scale production.

In the present paper, we describe the green hydrothermal synthesis of nest-like ZnO, without using the capping/structure directing agent. The as-synthesized ZnO nanostructures are evaluated against the commercial ZnO for their photocatalytic activities by using methylene blue (MB) as the model dye contaminant. The hierarchically structured nest-like ZnO show excellent photocatalytic activity for MB dye degradation.

### EXPERIMENTAL

#### 1. Synthesis of Nest-like ZnO

All chemicals were of analytical grade and used without further purification: zinc nitrate hexahydrate, zinc oxide (granular, surface area = 16 m<sup>2</sup>/g) and ammonium hydroxide were purchased from SdFine. Sodium hydroxide (Rankem), Methylene Blue (denoted as MB) (Fischer Scientific) and de-ionized water were employed for synthesis. The hydrothermal process was employed for the synthesis of ZnO sample as follows: Initially, 11 g zinc nitrate was dissolved in 100 mL of NH<sub>4</sub>OH. Then 4 g sodium hydroxide was added to the solution. After that, deionized water was added till the final concentration of the solution became 1 M Zn<sup>2+</sup> solution. This solution was then transferred to a Teflon lined autoclave and kept in an oven premaintained at 80 °C for 14 hours. The autoclave was cooled to room temperature naturally, the white precipitate so obtained was separated, washed for several times with de-ionized water, and twice

<sup>†</sup>To whom correspondence should be addressed.  
E-mail: sonalichaudhari5384@gmail.com

with ethanol and dried in oven at 60 °C for 12 hrs to get the nest-like ZnO powder.

## 2. Characterization

Powder X-ray diffraction patterns (XRD) were obtained on a diffractometer (Bruker Axs model D8 advance) with Cu K $\alpha$  radiation,  $\lambda=1.5418 \text{ \AA}$ . The morphologies of ZnO were obtained by a Hitachi S-4800 Field emission scanning electron microscope (FE-SEM). The Brunauer-Emmett-Teller method (BET) was employed to determine the surface area of samples by nitrogen gas adsorption in a Micromeritics ASAP2020M+C gas sorption analyzer. UV-visible absorption spectrum of as-synthesized ZnO product was recorded on a UV/Vis spectrophotometer (Perkin Elmer model Lamda 800). FTIR spectra of as-prepared purified ZnO powders were recorded using KBr pellets on a Perkin Elmer 1090 spectrometer. Raman spectra were measured with a Horiba Jobin Yvon LabRam IR system at a spatial resolution of 2 mm in a backscattering configuration. The 633-nm line of a Helium Neon laser was used as scattering light source with less than 4mW power. The photoluminescence spectrum of the ZnO sample in colloidal suspension was measured on a spectrofluorometer (JASCO model FP-6200) equipped with a Xenon lamp source, with an excitation wavelength of 325 nm.

## 3. Photodegradation of Methylene Blue (MB)

The photocatalytic activity experiments on the as-prepared nest-like ZnO nanostructures for the degradation of MB were performed at ambient temperature. A Pyrex beaker (250 mL) was used as the photoreactor. ZnO product as catalyst (0.05 g) was added in the aqueous MB solution ( $C_{16}H_{18}ClN_3S_3 \cdot 3H_2O$ ) (100 ppm, 100 mL), and the solution was magnetically stirred in the dark for 1 h to reach the adsorption equilibrium of MB with the catalyst and then exposed

to UV-light. At given irradiation time intervals, a series of aqueous solutions in a certain volume were collected and centrifuged to remove the catalysts and were then analyzed on a spectrophotometer. The concentration of methylene blue was determined by monitoring the changes in the main absorbance centered at 663 nm.

## RESULTS AND DISCUSSION

### 1. Morphology and Structure

Hierarchical nest-like ZnO nanostructures were prepared by simple hydrolysis of zinc nitrate with aqueous NaOH using hydrothermal method as described in the experimental section. The as-obtained ZnO nanostructures were examined with FESEM, XRD, Raman, PL, UV-vis absorption and BET surface area analysis. Fig. 1 shows the FESEM and XRD pattern of the as-prepared ZnO product. A panoramic morphology of the as-synthesized ZnO product is presented in Fig. 1(a). The image clearly shows the formation of well defined three-dimensional (3D) nest-like ZnO microstructures with diameters in the range 250-500 nm. These nest-like ZnO microstructures are very uniform and polydisperse in nature. It is interesting that we did not observe any other morphology rather than nests. A magnified FESEM image showing the close observation of these structures is presented in Fig. 1(b). It can be seen from the figure that the nest-like microstructures are assembled by many densely arranged nanosheets as “nest-walls”. A close up view of the nanosheets-built nest-like microstructure in Fig. 1(c) reveals that these nanosheets have thickness 10-25 nm and are grown sideways to the central wall to form many grooves. These grooves engendered in the 3D microstructures may improve the chemical properties or serve

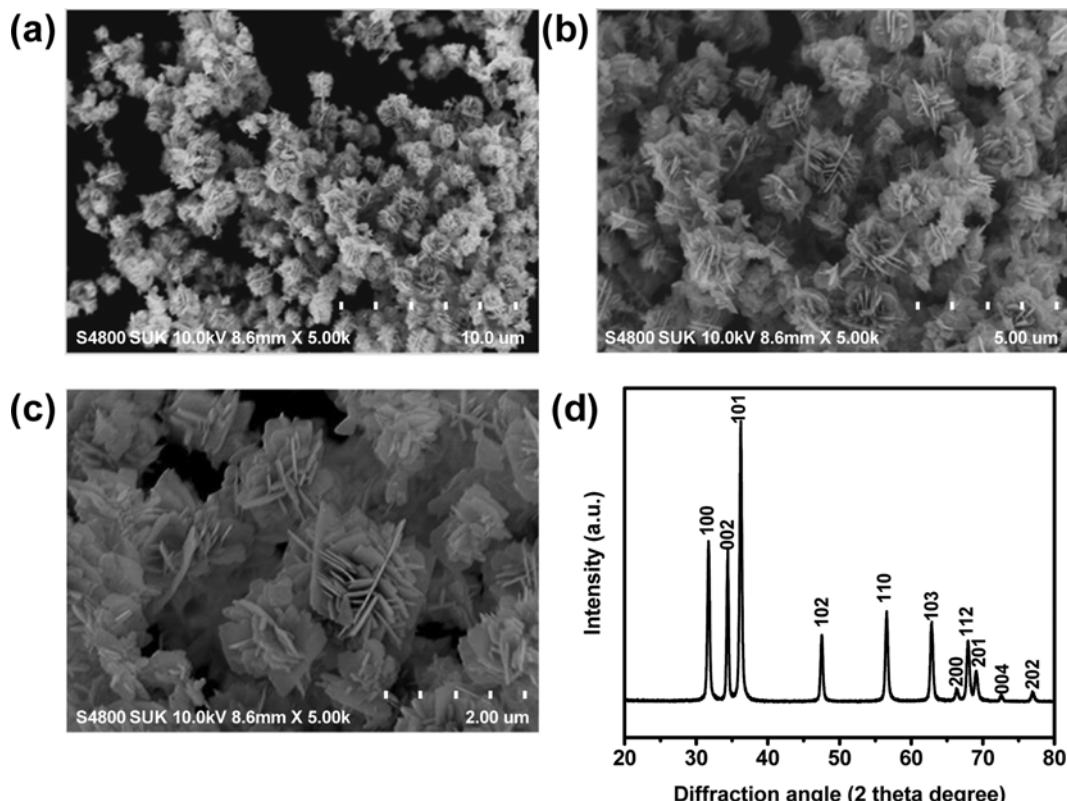


**Fig. 1. (a), (b) & (c) Panoramic and high resolution images and (d) X-ray diffraction pattern of nest-like ZnO.**

as transport paths for small molecules.

Regarding the formation of nest-like ZnO, the concentrations of  $Zn^{2+}$  and  $OH^-$  must have played key roles, since no template, organic additive, or surfactant existed in the synthetic architecture. For that reason, we suggest the following explanation for the formation of the 3D microstructures. It is well known that shape control of the crystals can be achieved by manipulating the growth kinetics. The crystal formation process is divided into two stages of nucleation and growth. The overall reaction for the growth of ZnO crystals may be expressed as follows:



In our present case, the contributing growth driving force for ZnO crystals is the concentration of  $Zn^{2+}$  ions. Initially, when  $Zn(NO_3)_2$  is introduced into  $NH_4OH$ , the solution becomes turbid due to formation of white  $Zn(OH)_2$  colloids (reaction (1) and (2)). At the same time, a part of  $NH_3$  can serve as the chelating agent to unite with  $Zn^{2+}$  to form the amine complex ( $Zn(NH_3)_4^{2+}$ ) according to reaction (3), which benefits from the generation of growth units ( $Zn(OH)_4^{2-}$ ). In the solution environment, a part of the  $Zn(OH)_2$  colloids dissolves onto  $Zn^{2+}$  and  $OH^-$  and large quantities of ZnO nuclei form when the concentration of  $Zn^{2+}$  and  $OH^-$  exceeds the critical value, and subsequent crystal growth develops (reactions (4) and (5)). As the reaction proceeds, the concentration of the  $Zn(OH)_4^{2-}$  becomes lower, and some active sites on the surface of initially formed ZnO aggregations grow along the oriented as the chemical environment constantly provides reactants.. The preferential growth along the [0001] and [0110] directions within the {2110} plane forms nanosheets on the surface of the initially formed ZnO aggregation. Subsequently, more and more nanosheets with a {2110}-planer surface are interlaced and overlapped with each other to form a multilayer

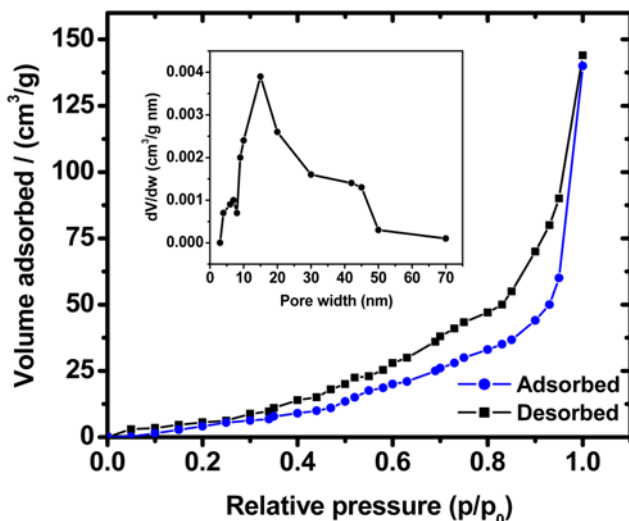


**Fig. 2.** The nitrogen adsorption-desorption isotherm of nest-like ZnO; pore size distribution curve of the nest-like ZnO (inset).

ered nest-like structure.

Fig. 1(d) shows the XRD pattern of as-synthesized nest-like ZnO sample. The diffraction peaks observed at  $2\theta=31.8, 34.5, 36.4, 47.5, 57.1, 63.2, 66.7, 67.8, 69, 72.6$ , and  $76.8^\circ$  match that of bulk wurtzite hexagonal ZnO having lattice constants of  $a$  and  $c$  equal to 3.25 and  $5.21\text{ \AA}^\circ$ , respectively (JCPDS file no. 36-1451). Note that no characteristic peaks corresponding to impurities, such as zinc hydroxide, were observed in the XRD pattern of any of the samples, which indicated the formation of pure ZnO nanostructures.

The nitrogen sorption isotherms of the synthesized nest-like ZnO sample were measured to gain information about the specific surface area and the pore sizes. As shown in Fig. 2, the nitrogen adsorption-desorption isotherms are identified as type IV, revealing the existence of abundant mesoporous structures in the architecture [37]. From the corresponding pore size distribution curve (shown in inset of Fig. 2), we find that the pore size distribution is not uniform, and most of the pores fall into the size ranging from 2 to 70 nm, which well agrees with the results of the FESEM analysis. Considering the observed morphology of the product, smaller pores with a peak at about 3 nm may be generated between primary nanocrystals, whereas the larger pores with a wide pore size distribution can be attributed to the spaces formed between the intercrossed ZnO nanosheets. The specific surface area of the as-synthesized nest-like ZnO is evaluated to be approximately  $25.2\text{ m}^2\text{g}^{-1}$  by BET equation, which is larger than that reported nanostructured ZnO [38] and the commercial one that is used as a comparative counterpart in this study. Obviously, this hierarchically structured ZnO with high surface area will be stable against aggregation, and may exhibit potential application in catalysis and sensing.

To identify the characteristic groups present on the surface of the ZnO samples that could react with the functional groups of other compounds, the zinc oxides were subjected to spectroscopic analysis. Fig. 3 depicts the FTIR spectrum of the as-synthesized nest-like ZnO nanostructures and the commercial ZnO sample used in the present study. It reveals a series of absorption peaks from  $500-4,000\text{ cm}^{-1}$ , and spectroscopic analysis confirmed previously published results [39,40]. The broad band at  $3,400\text{ cm}^{-1}$  is due to O-H stretching vibration of the hydroxyl group. Peaks at  $3,000\text{ cm}^{-1}$  and  $1,050\text{ cm}^{-1}$  are due to the C-H symmetric and asymmetric valency

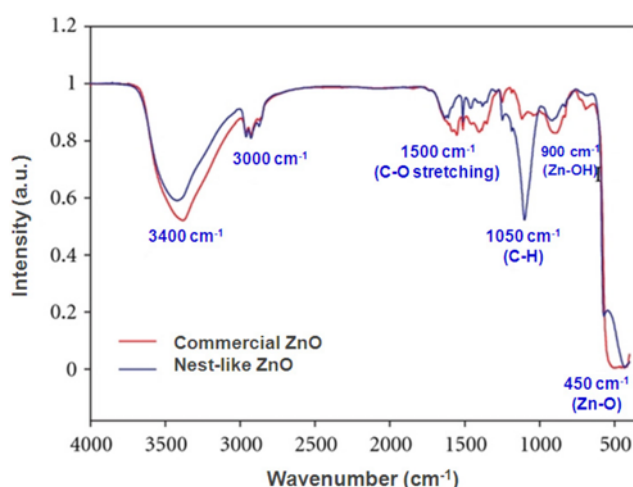


**Fig. 3.** FT-IR spectrum of nest-like and commercial ZnO.

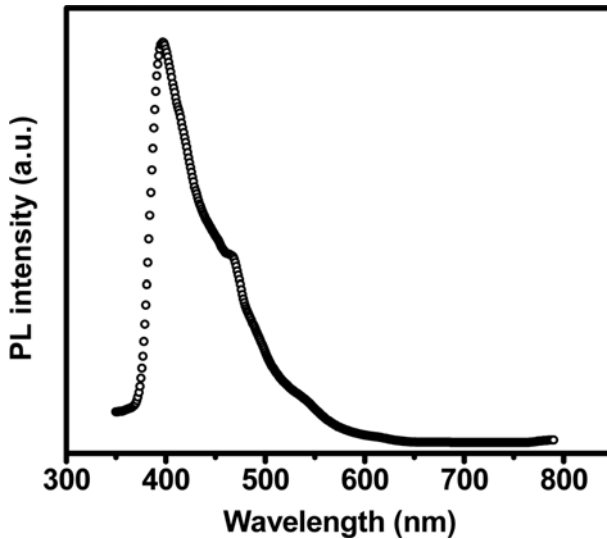


**Fig. 4. Photoluminescence (PL) spectrum of nest-like ZnO.**

bands. The peaks at  $1,300$  and  $1,500\text{ cm}^{-1}$  are due to stretching vibrations of C=O. The peaks corresponding to  $\nu_{\text{Zn-OH}}$ , and  $\nu_{\text{Zn-O}}$  appeared at  $900\text{ cm}^{-1}$  and  $450\text{ cm}^{-1}$ , respectively. The spectroscopic studies indirectly provide information about the surface character of the ZnO samples.

Generally, the PL spectrum of ZnO consists of three emission bands at room temperature, a near-band-edge (UV) emission and two broad, deep-level (visible) emissions. The visible emission is usually considered to be related to various intrinsic defects produced during ZnO preparation and post treatment. Normally, these defects are located on the surface of the ZnO structure. Fig. 4 presents the PL spectrum of the as-synthesized ZnO product excited at  $325\text{ nm}$  UV light from a He-Cd laser at room temperature. From the figure, a sharp UV emission peak at  $395\text{ nm}$  ( $\sim 3.13\text{ eV}$ ) and a green emission peak at  $460\text{ nm}$  ( $\sim 3.44\text{ eV}$ ) were observed in the PL spectrum. The emission at  $395\text{ nm}$  corresponds to the near band-edge emission resulting from the recombination of free excitons, whereas the negligible visible emission peaks at  $460\text{ nm}$  may be attributed to electron transition, mediated by defect levels in the band gap. It is established that the UV-emissions at  $390$ - $400\text{ nm}$  are attributed to UV emissions of Zn [41], reflecting a dominant good crystal. The blue green emission band at  $\sim 470\text{ nm}$  is related to the exciton scattering by some definite defects, usually attributed to a singly charged oxygen vacancy or other defects, which originate from the recombination of a photoexcited hole with a charge state of the specific defect, such as oxygen vacancies or it results from surface deep-traps [42]. The PL peak position and the relative intensity of band-edge emission to the deep-trap emission are closely related to the morphology, crystallinity, and dimension of ZnO structures. High band-edge emission indicates a high monocrystal structure, while dominant deep-trap emission reflects that numerous defects or oxygen vacancies or amorphous surface in ZnO crystal still influence the exciton transition. So, as-synthesized nest-like ZnO possesses good crystal structure and smooth crystal faces.

Room temperature Raman spectra were recorded using a Raman spectroscope with the Ar<sup>+</sup>-ion laser at  $488\text{ nm}$  that served as the excitation source. ZnO with wurtzite structure belongs to the  $C6V^4$

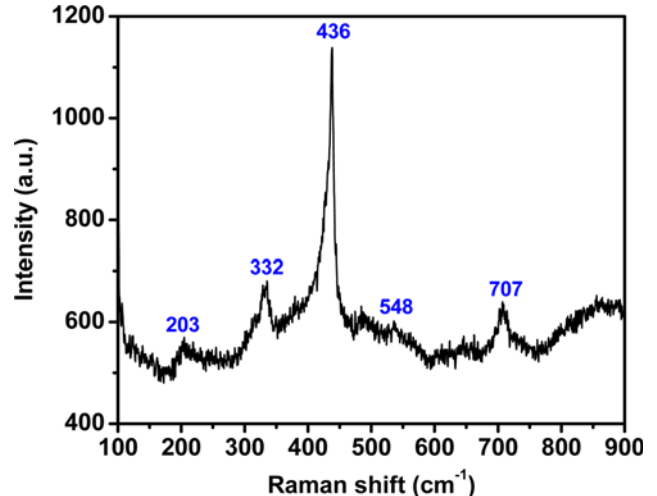


**Fig. 5. Room-temperature Raman spectrum of the nest-like ZnO.**

space group. At the  $\Gamma$  point of the Brillouin zone, optical phonons have the following irreducible representation:  $\Gamma_{\text{opt}}=\text{A}1+2\text{B}1+\text{E}1+2\text{E}2$  [43]. Among these, A1 and E1 modes are polar and can be split into transverse (TO) and longitudinal optical (LO) components, with all being Raman and infrared active. For the sample, vibration peaks can be clearly observed at  $203$ ,  $332$ ,  $436$ ,  $548$ , and  $707\text{ cm}^{-1}$  (Fig. 5). Among these peaks, the strongest one centered at about  $436\text{ cm}^{-1}$  is characteristic of the high-frequency E2 mode of the wurtzite structure. The peak at  $548\text{ cm}^{-1}$  corresponds to the LO phonon of A1 and E1, respectively. Besides these “classical” Raman modes, the Raman spectra also show other modes with frequencies of  $203$ ,  $332$ , and  $707\text{ cm}^{-1}$ . These additional peaks cannot be explained within the framework of the bulk single phonon modes, which are attributed to the multiphonon scattering processes [44].

## 2. Photocatalytic Activity

Fig. 6(a) displays the UV-visible absorption spectra changes of the MB solution during degradation with as synthesized nest-like ZnO. For nest-like ZnO sample, with the extension of the exposure time, the intensity of MB characteristic absorption peak decreases evidently, indicating that MB molecule is degraded gradually. Fig. 6(b) shows a comparison of the degradation rates of MB over commercial and nest-like ZnO and in absence of photocatalyst under identical conditions ( $C_0$  and  $C$  being the equilibrium concentration of MB before and after UV irradiation, respectively). In absence of catalyst, only a slight decrease in the concentration of MB is detected in presence of UV irradiation for 150 mins. In the presence of UV irradiation the commercial and as-synthesized nest-like ZnO degraded MB solution to  $79.98\%$  and  $95.34\%$ , respectively. Obviously, the photocatalytic efficiency of nest-like ZnO is much better than that of its commercial counterpart. Further, the experimental data of the photocatalytic process is illustrated by the pseudo-first-order kinetics simulation. As shown in Fig. 6(c), the photodegradation rate constants for nest-like and commercial ZnO samples are found to be  $0.064\text{ min}^{-1}$  and  $0.014\text{ min}^{-1}$ , respectively, so the degradation rate of nest-like ZnO is more than that of the commercial one. Compared with commercial ZnO, nest-like ZnO possesses the smaller size and higher specific surface area, which will enhance the contact between the catalyst and MB dye molecules because the photocat-

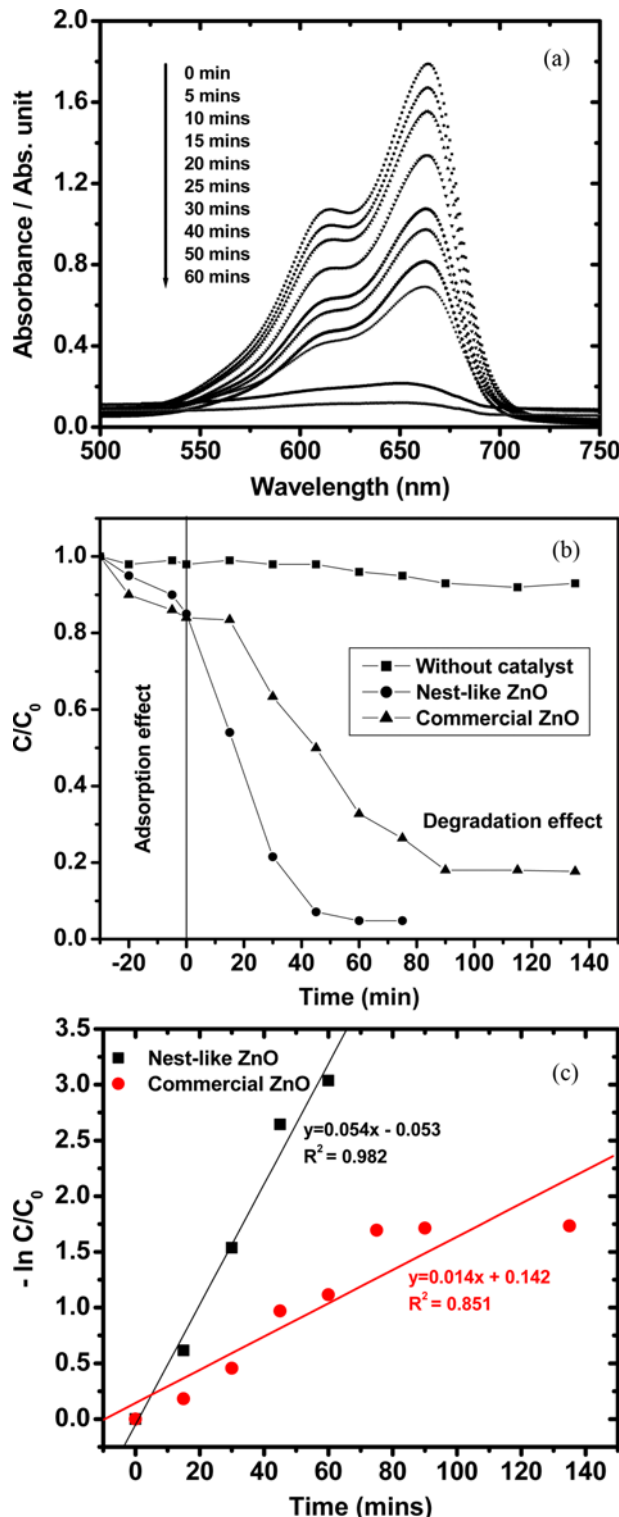


Fig. 6. (a) Time dependent UV-vis absorption spectra of the MB dye aqueous solution in presence of nest-like ZnO, (b) Photocatalytic efficiency  $c/c_0$  of MB solution in presence of nest-like and commercial ZnO versus irradiation time, (c) Kinetics of the MB degradation photocatalyzed by nest-like and commercial ZnO.

alytic process usually occurs at the surface of the catalyst. Moreover, due to the larger specific surface area, more photogenerated

electron-hole pairs will be formed on the surface under UV irradiation, and hence the more effective holes and the more reactive sites formed for the MB molecule, which accelerates the reaction rate and thus promotes the degradation efficiency markedly.

Chakrabarti et al. [45] reported the photocatalytic degradation of model textile dyes, Methylene Blue and Eosin Y, in wastewater using ZnO as semiconductor catalyst under UV-irradiation. Recently, Tak et al. [46] reported the CdS nanoparticles coupled ZnO with enhanced photocatalytic activity compared to as-synthesized bare ZnO. Further, dumbbell-shaped ZnO microcrystal photocatalyst was reported by Sun et al. [47], and the photocatalytic activity of the prepared dumbbell-shaped ZnO microcrystal photocatalyst was evaluated by the degradation of three different kinds of dye wastewater (Crystal Violet, Methyl Violet and Methylene Blue). After 75 min reaction, the decolorization efficiencies of the three kinds of dyes wastewater achieved was found to be 68.0%, 99.0% and 98.5%, respectively. In comparison of the above reported results, our nest-like ZnO catalyst prepared at relatively low hydrothermal temperature (800°C) has advantages of operating without the assistance of any semiconductor sensitizer and with comparable photocatalytic activity of degrading 95% Methylene blue (100 ppm, 100 ml) dye solution along with 0.5 gm of catalyst within 60 mins, and it could be considered as a promising photocatalyst for dye wastewater treatment.

## CONCLUSIONS

3D porous nest-like ZnO nanostructures have been fabricated by a simple hydrothermal process operated at ambient temperature (80 °C). The as-obtained ZnO nanostructures are composed of numerous nanosheets which endow many grooves in the nanostructures. These grooves are mainly responsible for improved catalytic activities. The photocatalytic measurement demonstrated that the nest-like ZnO possesses excellent photocatalytic activities for degradation of MB dye.

## REFERENCES

- H. Morkoc and U. Ozgur, *Zinc oxide: Fundamentals, materials and device technology*, Wiley, Germany, **1**, 246 (2009).
- S. Sakthivel, B. Neppolian, M. V. Shankar, B. Arabindoo, M. Palanichamy and V. Murugesan, *Sol. Energy Mater. Sol. C*, **77**, 65 (2003).
- H. Hidaka, K. Nohara, K. Ooishi, J. Zhao, N. Serpone and E. Pelizzetti, *Chemosphere*, **29**, 2619 (1994).
- K. Hayat, M. A. Gondal, M. M. Khaled, Sh. Ahmed and A. M. Shemsi, *Appl. Catal. A-Gen.*, **393**, 122 (2011).
- S. Anandan, A. Vinu, T. Mori, N. Gokulakrishnan, P. Srinivasu, V. Murugesan and K. Ariga, *Catal. Commun.*, **8**, 1377 (2007).
- H. Yan and J. Hou, *Mater. Res. Bull.*, **44**, 1954 (2009).
- S. K. Pardeshi and A. B. Patil, *J. Hazard. Mater.*, **163**, 403 (2009).
- T. Ootsuka, Z. Liu, M. Osamura, Y. Fukuzawa, R. Kuroda and Y. Suzuki, *Thin Solid Films*, **476**, 30 (2005).
- H. M. Cheng, W.-H. Chiu, C.-H. Lee, S.-Y. Tsai and W.-F. Hsieh, *J. Phys. Chem. C*, **112**, 16359 (2008).
- D. C. Reynolds, D. C. Look, B. Jogai and H. Morkoc, *Solid State Commun.*, **101**, 643 (1997).
- D. C. Look, *Mater. Sci. Eng. B*, **80**, 383 (2001).

12. J. Muller and S. W. Fresenius, *J. Anal. Chem.*, **394**, 380 (1994).
13. H. Kind, H. Q. Yan, M. Law, B. Messer and P. D. Yang, *Adv. Mater.*, **14**, 158 (2002).
14. M. H. Huang, S. Mao, H. Feick, H. Q. Yan, Y. Y. Wu, H. Kind, E. Weber, R. Russo and P. D. Yang, *Science*, **292**, 1897 (2001).
15. S. S. Hullavarad, N. V. Hullavarad, P. C. Karulkar, A. Luykx and P. Valdivia, *Nanoscale Res. Lett.*, **2**, 161 (2007).
16. S. J. Henley, M. N. R. Ashfold and D. Cherns, *Surf. Coat. Technol.*, **177**, 271 (2004).
17. Y. Zheng, C. Chen, Y. Zhan, X. Lin, Q. Zheng, K. Wei, J. Zhu and Y. Zhu, *Inorg. Chem.*, **46**, 6675 (2007).
18. R. Jalal, E. K. Goharshadi, M. Abareshia, M. Moosavi, A. Yousefi and P. Nancarrow, *Mater. Chem. Phys.*, **121**, 198 (2010).
19. N. K. Zayer, R. Greef, K. Rogers, A. J. C. Grellier and C. N. Pannell, *Thin Solid Films*, **352**, 179 (1999).
20. C. X. Xu and X. W. Sun, *Appl. Phys. Lett.*, **83**, 3806 (2003).
21. A. Dev, S. Kar, S. Chakrabarti and S. Chaudhuri, *Nanotechnology*, **17**, 1533 (2006).
22. A. Wei, X. W. Sun, C. X. Xu, Z. L. Dong, M. B. Yu and W. Huang, *Appl. Phys. Lett.*, **88**, 213102 (2006).
23. L. Liao, J. C. Li, D. F. Wang, C. Liu and Q. Fu, *Appl. Phys. Lett.*, **86**, 083106 (2005).
24. C. Wang, E. Wang, E. Shen, L. Gao, Z. Kang, C. Tian, C. Zhang and Y. Lan, *Mater. Res. Bull.*, **41**, 2298 (2006).
25. Z. Wang, X. F. Qian, J. Yin and Z. K. Zhu, *J. Solid State Chem.*, **177**, 2144 (2004).
26. Z. Wang, X. F. Qian, J. Yin and Z. K. Zhu, *Langmuir*, **20**, 3441 (2004).
27. Z. W. Pan, Z. R. Dai and Z. L. Wang, *Science*, **291**, 1947 (2001).
28. X. H. Kong, X. M. Sun, X. L. Li and Y. D. Li, *Mater. Chem. Phys.*, **82**, 997 (2003).
29. K. Tominaga, T. Takao, A. Fukushima, T. Moriga and I. Nakabayashi, *Vacuum*, **66**, 505 (2002).
30. N. Naghavi, C. Marcel, L. Dupont, A. Rougier, J. B. Leriche and C. Guery, *J. Mater. Chem.*, **10**, 2315 (2000).
31. P. Yang, H. Yan and S. Mao, *Adv. Funct. Mater.*, **12**, 323 (2002).
32. Y. Feng, Y. Zhou, Y. Liu, G. Zhang and X. Zhang, *J. Lumin.*, **120**, 233 (2006).
33. H.-J. Zhai, W.-H. Wu, F. Lu, H.-S. Wang and C. Wang, *Mater. Chem. Phys.*, **112**, 1024 (2008).
34. P. Sagar, P. K. Shishodia, R. M. Mehra, H. Okada, A. Wakahara and A. Yoshida, *J. Lumin.*, **126**, 800 (2007).
35. R. V. Kumar, Y. Diamant and A. Gedanken, *Chem. Mater.*, **12**, 2301 (2000).
36. B. X. Lin, Z. X. Fu and Y. B. Jia, *Appl. Phys. Lett.*, **79**, 943 (2001).
37. J. Y. Chen, T. Herricks, M. Geissler and Y. N. Xia, *J. Am. Chem. Soc.*, **126**, 10854 (2004).
38. J. S. Hu, L. L. Ren, Y. G. Guo, H. P. Liang, A. M. Cao, L. J. Wan and C. L. Bai, *Angew. Chem. Int. Ed.*, **44**, 1269 (2005).
39. S. Bhattacharyya and A. Gedanken, *Micropor. Mesopor. Mater.*, **110**, 553 (2008).
40. E. Tang, G. Cheng and X. Ma, *Powder Technol.*, **161**, 209 (2006).
41. B. Zou, R. Liu, F. Wang, A. Pan, L. Cao and Z. L. Wang, *J. Phys. Chem. B*, **110**, 12865 (2006).
42. C. Li, G. Hong, P. Wang, D. Yu and L. Qi, *Chem. Mater.*, **21**, 891 (2009).
43. F. Decremps, J. P. Porres, A. M. Saitta, J. C. Chervin and A. Polian, *Phys. Rev. B*, **65**, 092101 (2002).
44. R. B. Liu, A. L. Pan, H. M. Fan, F. F. Wang, Z. X. Shen, G. Z. Yang, S. S. Xie and B. J. Zou, *Phys.: Condens. Matter.*, **19**, 136206 (2007).
45. S. Chakrabarti and B. K. Dutta, *J. Haz. Mat.*, **112**, 269 (2004).
46. Y. Tak, H. Kim, D. Lee and K. Yong, *Chem. Commun.*, **38**, 4585 (2008).
47. J.-H. Sun, S.-Y. Dong, Y.-K. Wang and S.-P. Sun, *J. Hazard. Mater.*, **172**, 1520 (2009).